Journal of Basics and Applied Sciences Research (JOBASR)
ISSN (print): 3026-9091, ISSN (online): 1597-9962
Volume 4(3) May 2026
DOI: https://dx.doi.org/10.4314/jobasr.v4i3.24

Finite-Size Scaling and Interaction-Range Renormalization of Critical Phenomena in a Three-Dimensional Lennard–Jones Fluid

Isaiah Eze Igwe[1*]
[1]**Department of Physics, Federal University Dutsin-Ma, Katsina State**
[*]Corresponding Author Email: iigwe@fudutsinma.edu.ng

ABSTRACT
Finite-size effects and interaction-range truncation remain major challenges in accurately determining critical properties from Molecular Dynamics simulations of fluids. Here, the critical behavior of a three-dimensional Lennard–Jones fluid was investigated using Molecular Dynamics simulations combined with finite-size scaling, Binder cumulants, correlation-length analysis, and dynamic criticality measurements. Simulations were performed for system sizes ranging from $(N = 500)$ to 4000 particles and cutoff radii from $r_c = 2.5\sigma$ to 4.0σ. As the vapor–liquid critical region was approached, the local-density susceptibility increased by more than a factor of three, while the correlation length grew from approximately (2σ) to over (12σ), indicating the emergence of long-range density fluctuations. Finite-size extrapolation yielded thermodynamic-limit critical parameters of $(T_c \approx 1.22)$ and $(\rho_c \approx 0.31)$, in close agreement with established Lennard–Jones reference values. Dynamic analyses revealed pronounced critical slowing down, with relaxation times increasing by nearly an order of magnitude near criticality. Increasing the cutoff radius systematically shifted the critical temperature upward by approximately $5–6\%$ and enhanced susceptibility amplitudes. A near-linear relationship was observed between the critical-temperature shift and the omitted tail energy, leading to the development of a unified energetic scaling framework based on the cumulative attraction parameter $(\lambda(r_c))$. The resulting universal renormalization curve establishes a direct microscopic-to-macroscopic connection between interaction truncation, fluctuation growth, and emergent critical behavior in finite molecular systems.

Keywords:
Lennard–Jones fluid;
Finite-size scaling;
Critical phenomena;
Critical slowing down;
Renormalization

INTRODUCTION

Critical phenomena continue to occupy a central position in statistical mechanics because they provide one of the clearest manifestations of how microscopic interactions generate emergent macroscopic behavior. Near a critical point, thermodynamic response functions become strongly enhanced, density fluctuations span multiple length scales, and the distinction between microscopic and macroscopic descriptions becomes increasingly blurred (Mouritsen, 1989; Nishimori, Ortiz, Nishimori, & Ortiz, 2010). Although the universal features of criticality are now well established theoretically, extracting critical behavior from finite computational systems remains a nontrivial challenge. The problem is particularly relevant for molecular simulations, where finite particle numbers, finite simulation volumes, interaction truncation, and limited sampling times may all influence the apparent critical behavior observed in practice (Binder, 1981; Landau, 2014; Privman, 1990).

Among the many model systems used to investigate critical phenomena, the Lennard–Jones (LJ) fluid occupies a unique position. Despite its simple pairwise interaction potential, $U(r) = 4\varepsilon\left[\left(\frac{\sigma}{r}\right)^{12} - \left(\frac{\sigma}{r}\right)^{6}\right]$, the model reproduces many of the essential thermodynamic properties of simple atomic fluids, including vapor–liquid coexistence, surface tension, phase separation, and critical behavior (Hansen & McDonald, 2013; Jones, 1924; Rowlinson & Widom, 2002). For nearly a century, the LJ fluid has served as a benchmark for testing theoretical developments, simulation methodologies, and equations of state (Johnson, Zollweg, & Gubbins, 1993; Thol et al., 2016; Verlet, 1967). It is difficult to think of another continuous fluid model that has been scrutinized as extensively. Yet the apparent maturity of LJ-fluid research can sometimes be misleading. Accurate determination of critical parameters remains remarkably sensitive to methodological choices. Small variations in system size, cutoff treatment, ensemble selection,

How to cite this article: Isaiah E. I. (2026). Finite-Size Scaling and Interaction-Range Renormalization of Critical Phenomena in a Three-Dimensional Lennard–Jones Fluid. *Journal of Basics and Applied Sciences Research*, *4*(3), 223-240. https://dx.doi.org/10.4314/jobasr.v4i3.24

or sampling protocol may shift the estimated critical temperature and density by amounts that are not negligible when finite-size scaling analyses are performed (Caillol, 1998; Potoff & Panagiotopoulos, 1998; Smit, 1992; Wilding, 1995). In other words, the critical point is not merely a thermodynamic property to be measured; it is also a stringent test of how faithfully simulations reproduce long-range fluctuation physics.

Historically, most high-precision investigations of LJ criticality have relied on Monte Carlo techniques. The pioneering work of Wilding (Wilding, 1995) demonstrated that mixed-field finite-size scaling could be used to obtain highly accurate estimates of the LJ critical point while simultaneously confirming consistency with the three-dimensional Ising universality class. Similar approaches were later refined by Bruce and Wilding (Bruce & Wilding, 1992), Potoff and Panagiotopoulos (Potoff & Panagiotopoulos, 1998), among others. These studies transformed understanding of fluid criticality by adapting finite-size scaling concepts originally developed for magnetic systems to asymmetric fluids. Subsequent analyses further clarified the importance of field mixing, order-parameter distributions, and histogram reweighting techniques in extracting critical behavior from finite systems(Bruce & Wilding, 1992; Fisher & Barber, 1972; Kim, Fisher, & Luijten, 2003; Wilding, 1995). A common feature of much of this literature is the dominant role played by grand-canonical and Monte Carlo methodologies. This preference is understandable. Critical phenomena are fluctuation dominated, and Monte Carlo methods are particularly well suited for sampling equilibrium distributions near phase transitions (Frenkel & Smit, 2023; Landau, 2014; Smit, 1992). Molecular Dynamics (MD), by contrast, has often been viewed primarily as a tool for studying transport processes, structural relaxation, and time-dependent behavior. As a result, finite-size scaling studies based explicitly on MD trajectories remain comparatively less common. This situation raises an interesting question. To what extent can critical behavior be recovered directly from Molecular Dynamics simulations? The question may appear straightforward, but it is not. Canonical MD simulations operate under fixed particle number, volume, and temperature conditions. Consequently, global density fluctuations, which are central to many descriptions of criticality, are constrained by construction. A finite NVT system cannot exhibit the same fluctuation spectrum as a grand-canonical system, regardless of simulation length (Allen & Tildesley, 2017; Hansen & McDonald, 2013; Torquato & Stillinger, 2003). This limitation does not imply that MD is unsuitable for critical studies. Rather, it suggests that alternative observables may be required if critical behavior is to be characterized reliably from trajectory-based simulations.

Recent developments point toward several possibilities. Local density fluctuations, coarse-grained order parameters, Binder cumulants, cluster statistics, and spatial correlation functions have emerged as useful tools for identifying critical signatures even in ensembles where global density is constrained (Binder, 1981; Egami, 2020; Kim et al., 2003). At the same time, MD provides direct access to dynamic information unavailable from conventional equilibrium Monte Carlo simulations. Density autocorrelation functions, relaxation times, and critical slowing-down behavior can all be obtained naturally from particle trajectories (Das, Fisher, Sengers, Horbach, & Binder, 2006; Das, Roy, & Midya, 2015; Onuki, 2002). These dynamic observables may provide complementary insights into criticality that remain difficult to access through purely equilibrium approaches. Another issue that deserves closer examination concerns the treatment of intermolecular interactions. Nearly all practical LJ simulations truncate the potential at a finite cutoff radius. While this procedure improves computational efficiency, it also modifies the effective thermodynamic model being simulated (Allen & Tildesley, 2017; Smit, 1992). Earlier studies have shown that critical parameters depend on cutoff treatment, particularly when long-range attractive interactions are neglected or incompletely corrected (Caillol, 1998; Janeček, 2006; Smit, 1992). The problem becomes especially relevant in finite-size scaling analyses because the effects of truncation and finite system size may become intertwined. A finite system already suppresses long-wavelength fluctuations; reducing the interaction range introduces an additional modification to the fluctuation spectrum. Distinguishing between these two effects is not always straightforward.

Interestingly, most finite-size scaling studies focus on either finite-size effects or interaction-range effects, but rarely on their combined influence. High-accuracy critical-point studies often assume a fixed potential treatment and then investigate finite-size corrections within that framework (Kim et al., 2003; Potoff & Panagiotopoulos, 1998; Wilding, 1995). Conversely, studies examining cutoff dependence frequently focus on coexistence properties or equations of state rather than scaling behavior itself (Johnson et al., 1993; Smit, 1992; Thol et al., 2016). As a result, a gap remains in understanding how cutoff treatment influences finite-size scaling signatures extracted from MD simulations near criticality. A related issue concerns reproducibility. Modern molecular simulation studies increasingly emphasize transparent workflows, statistical uncertainty quantification, and reproducible computational protocols (Grossfield et al., 2018; Plimpton, 1995; Thompson et al., 2022). Critical phenomena present a particularly demanding test because equilibration times increase dramatically near the critical region. Apparent critical fluctuations may sometimes reflect inadequate equilibration, finite sampling windows, or metastable phase-separated configurations rather than genuine

critical behavior. Without careful analysis, it can be difficult to distinguish physical signals from simulation artifacts.

The present study is motivated by these considerations. Rather than attempting to compete with the highest-precision Monte Carlo estimates of LJ critical parameters, the objective is different. The aim is to examine what finite-size scaling information can be extracted from systematically designed Molecular Dynamics simulations and to evaluate how system size and cutoff treatment influence the resulting critical signatures. Particular attention is given to local density fluctuations, finite-size shifts in apparent critical temperatures, Binder-type cumulants, and dynamic relaxation behavior. By combining static and dynamic observables within a unified MD framework, the study seeks to clarify which aspects of criticality can be reliably recovered from trajectory-based simulations and which remain strongly influenced by finite-size or methodological constraints. Three working hypotheses guide the investigation. First, the apparent critical temperature is expected to exhibit finite-size shifts consistent with scaling theory, although the amplitudes of these shifts may depend on cutoff treatment. Second, local density fluctuation measures are anticipated to provide more reliable critical indicators than global density observables in NVT simulations. Third, dynamic relaxation times are expected to increase systematically with system size near the critical region, reflecting signatures of critical slowing down. Testing these hypotheses provides a framework for linking equilibrium finite-size scaling with time-dependent MD observables.

Accordingly, the aim of this work is to investigate finite-size scaling behavior in a three-dimensional Lennard–Jones fluid using Molecular Dynamics simulations, with emphasis on the combined influence of system size, interaction cutoff, and density fluctuations on apparent critical behavior. Specifically, the study seeks to: (i) perform MD simulations across multiple system sizes and temperatures near the vapor–liquid critical region; (ii) quantify finite-size effects on thermodynamic and fluctuation-based observables; (iii) estimate finite-size critical parameters and their scaling behavior; (iv) evaluate the influence of interaction truncation on critical signatures; and (v) characterize dynamic critical behavior through density relaxation and autocorrelation analyses. By addressing these objectives, the present work contributes to an area that remains somewhat underexplored relative to the extensive Monte Carlo literature. The emphasis is not solely on locating a critical point, but on understanding how finite-size effects, interaction truncation, and trajectory-based observables collectively shape the interpretation of critical behavior in Molecular Dynamics simulations of simple fluids.

MATERIALS AND METHODS

Theoretical Framework

The vapor-liquid critical behavior of simple fluids emerges from collective intermolecular interactions operating over multiple length scales. As the critical point is approached, thermodynamic fluctuations increase substantially and the correlation length grows until it becomes comparable to the dimensions of the simulation box. Under such conditions, finite-size effects become unavoidable and the apparent critical behavior depends explicitly on system size (Binder, 1981; Fisher & Barber, 1972; Privman, 1990).

The present study employs the Lennard-Jones (LJ) fluid as a model system. The pair interaction potential is given by

$$U(r) = 4\varepsilon\left[\left(\frac{\sigma}{r}\right)^{12} - \left(\frac{\sigma}{r}\right)^{6}\right] \quad (1)$$

where r is the intermolecular separation distance, ε is the characteristic interaction energy, and σ is the molecular diameter (Jones, 1924). The first term represents short-range repulsion arising from electron cloud overlap, whereas the second term accounts for long-range attractive dispersion forces. Despite its simplicity, the LJ potential reproduces the essential phase behavior of simple fluids, including vapor-liquid coexistence and criticality (Hansen & McDonald, 2013).

Reduced Lennard-Jones Units

To facilitate comparison with previous studies, all quantities were expressed in reduced LJ units: $\sigma = 1$; $\varepsilon = 1$; $m = 1$; $k_B = 1$. The reduced temperature, density, pressure, and time are therefore $T^* = \frac{k_B T}{\varepsilon}$; $\rho^* = \rho\sigma^3$; $P^* = \frac{P\sigma^3}{\varepsilon}$; $t^* = t\sqrt{\frac{\varepsilon}{m\sigma^2}}$ where $k_B T$ is Boltzmann's constant and m is the particle mass.

Virial Formulation of Pressure

Pressure was evaluated using the virial theorem:

$$P = \rho k_B T + \frac{1}{3V}\left\langle \sum_{i<j} r_{ij} \,.\, F_{ij} \right\rangle \quad (2)$$

Where P = system pressure, ρ = number density, V = simulation volume, r_{ij} = separation vector between particles i and j, F_{ij} = force acting between particles i and j. The first term represents the kinetic contribution, while the second term accounts for intermolecular interactions. Near the critical region, fluctuations in the configurational virial term become increasingly important because they reflect large-scale density fluctuations.

Compressibility and Density Fluctuations

The isothermal compressibility is defined as

$$\kappa_T = \frac{1}{\rho}\left(\frac{\partial \rho}{\partial P}\right)_T \quad (3)$$

In the thermodynamic limit, κ_T diverges at the critical point. In finite systems, however, the divergence is replaced by a finite maximum whose position depends on

system size (Binder, 1981). To quantify density fluctuations, the local susceptibility was computed from

$$\chi_\rho = \frac{V_l}{k_B T} \left(\langle \rho^2 l \rangle - \langle \rho l \rangle^2\right) \quad (4)$$

Where ρl = local density, V_l = subvolume used for coarse-graining. This quantity serves as the fluid analogue of magnetic susceptibility in spin systems.

Binder Cumulant Analysis

To identify finite-size critical behavior, the fourth-order Binder cumulant was evaluated using

$$U_4 = 1 - \frac{\langle m^4 \rangle}{3\langle m^2 \rangle^2} \quad (5)$$

Where $m = \rho l - \langle \rho l \rangle$ is the fluctuation of the local density about its mean value. For systems exhibiting universal critical behavior, Binder cumulant curves corresponding to different system sizes tend to intersect near the critical temperature (Binder, 1981; Landau, 2014).

Finite-Size Scaling Relations

Finite-size scaling predicts that the apparent critical temperature varies with box length according to

$$T_c(L) = T_c(\infty) + aL^{-\frac{1}{\nu}} \quad (6)$$

Where $T_c(L)$ = finite-system critical temperature, $T_c(\infty)$ = thermodynamic-limit critical temperature, a = non-universal amplitude, ν = correlation length exponent. For the three-dimensional Ising universality class,

$$\nu \approx 0.630, \quad \beta \approx 0.326, \quad \gamma \approx 1.237 \quad (7)$$

where β and γ are the order-parameter and susceptibility critical exponents, respectively. The order parameter obeys

$$M(L, T_c) \propto L^{-\frac{\beta}{\nu}} \quad (8)$$

while the susceptibility scales as $\chi(L, Tc) \propto L^{\gamma/\nu}$. These scaling relations were used to determine whether the simulation results are consistent with Ising-like critical behavior.

Dynamic Critical Behavior

One advantage of Molecular Dynamics simulations is direct access to time-dependent fluctuations. The normalized density autocorrelation function was computed as

$$C_\rho(t) = \frac{\langle \delta\rho(0)\delta\rho(t) \rangle}{\langle \delta\rho^2 \rangle} \quad (9)$$

Where $\delta\rho(t) = \rho(t) - \langle \rho \rangle$. The corresponding relaxation time was obtained from $\tau = \int C_\rho(t)dt$. As the critical region is approached, τ is expected to increase significantly because of critical slowing down (Das et al., 2006; Onuki, 2002).

Computational Procedure

All Molecular Dynamics simulations were carried out using the Large-scale Atomic/Molecular Massively Parallel Simulator (LAMMPS) package (Aug02 2023version) (Thompson et al., 2022). Periodic boundary conditions were applied in all three spatial directions to minimize surface effects.

System Initialization

Particles were initially arranged on a face-centered cubic (FCC) lattice and assigned Maxwell-Boltzmann velocity distributions corresponding to the target reduced temperature. To investigate finite-size effects, six system sizes were considered: N = 500, 864, 1372, 2048, 4000, and 6912 particles. The simulation box length was determined from $L = \left(\frac{N}{\rho}\right)^{1/3}$ for each density investigated.

Thermodynamic Conditions

The simulations focused on the vicinity of the vapor-liquid critical region. Reduced temperatures examined were $T^* = 1.20, 1.24, 1.26, 1.28, 1.30, 1.32, 1.34, 1.36,$ and 1.40. Reduced densities ranged between $0.20 \leq \rho^* \leq 0.40$.

Cutoff Treatment

To evaluate interaction-range effects, three cutoff radii were employed: $r_c = 2.5\sigma, 3.0\sigma$ and 4.0σ. For each cutoff radius, simulations were performed both with and without analytical long-range tail corrections. The energy correction per particle is

$$\frac{U_{tail}}{N} = 8\pi\rho\varepsilon\sigma^3 \left[\frac{1}{9}\left(\frac{\sigma}{r_c}\right)^9 - \frac{1}{3}\left(\frac{\sigma}{r_c}\right)^3\right] \quad (10)$$

while the pressure correction is

$$P_{tail} = \frac{16\pi}{3}\rho^2\varepsilon\sigma^3 \left[\frac{2}{3}\left(\frac{\sigma}{r_c}\right)^9 - \left(\frac{\sigma}{r_c}\right)^3\right] \quad (11)$$

Integration and Sampling

The equations of motion were integrated using the velocity-Verlet algorithm with a timestep $\Delta t * = 0.005$. Temperature control was achieved using a Nosé-Hoover thermostat. Each state point was equilibrated for 2×10^5 timesteps, followed by production runs of 1×10^6 timesteps. For temperatures closest to the critical region, production trajectories were extended to 5×10^6 timesteps to ensure adequate sampling of long-lived fluctuations.

Statistical Analysis

Block averaging was employed to estimate statistical uncertainties and reduce correlation effects between successive configurations (Allen & Tildesley, 2017). Independent simulations with different initial velocity seeds were performed for each state point. Reported values correspond to averages over independent trajectories, while uncertainties represent one standard deviation of the mean.

Equilibration and Thermodynamic Stability Near the Critical Region

Before examining finite-size scaling behavior, it is necessary to establish that the simulated systems reached thermodynamic equilibrium and that the measured fluctuations reflect equilibrium critical phenomena rather than transient relaxation effects. This requirement becomes particularly important near the vapor–liquid critical point because relaxation times increase substantially as the correlation length grows, leading to the phenomenon of critical slowing down (Binder, 1981; Onuki, 2002). In finite systems, inadequate equilibration can easily masquerade as critical behavior, especially when density fluctuations become long-lived and heterogeneous. Figure 1 summarizes the equilibration behavior of representative Lennard–Jones systems through the temporal evolution of reduced temperature, virial pressure, potential energy, and three-dimensional particle configurations. Following initialization from a face-centered cubic lattice, all systems underwent rapid structural relaxation during the first $10^4 - 10^5$ timesteps. Subsequently, the monitored thermodynamic observables fluctuated around stationary mean values without exhibiting systematic drift. The reduced temperature shown in Fig. 1(a) converged rapidly toward the target thermostat value and remained stable throughout the production stage. The fluctuations observed after equilibration were small and statistically symmetric about the mean. Such behavior confirms that the selected timestep $\Delta t^* = 0.005$ is sufficiently small to ensure numerical stability while maintaining computational efficiency. Similar equilibration characteristics have been reported in previous Molecular Dynamics studies of Lennard–Jones fluids employing velocity-Verlet integration and Nosé–Hoover thermostatting (Allen & Tildesley, 2017; Frenkel & Smit, 2023).

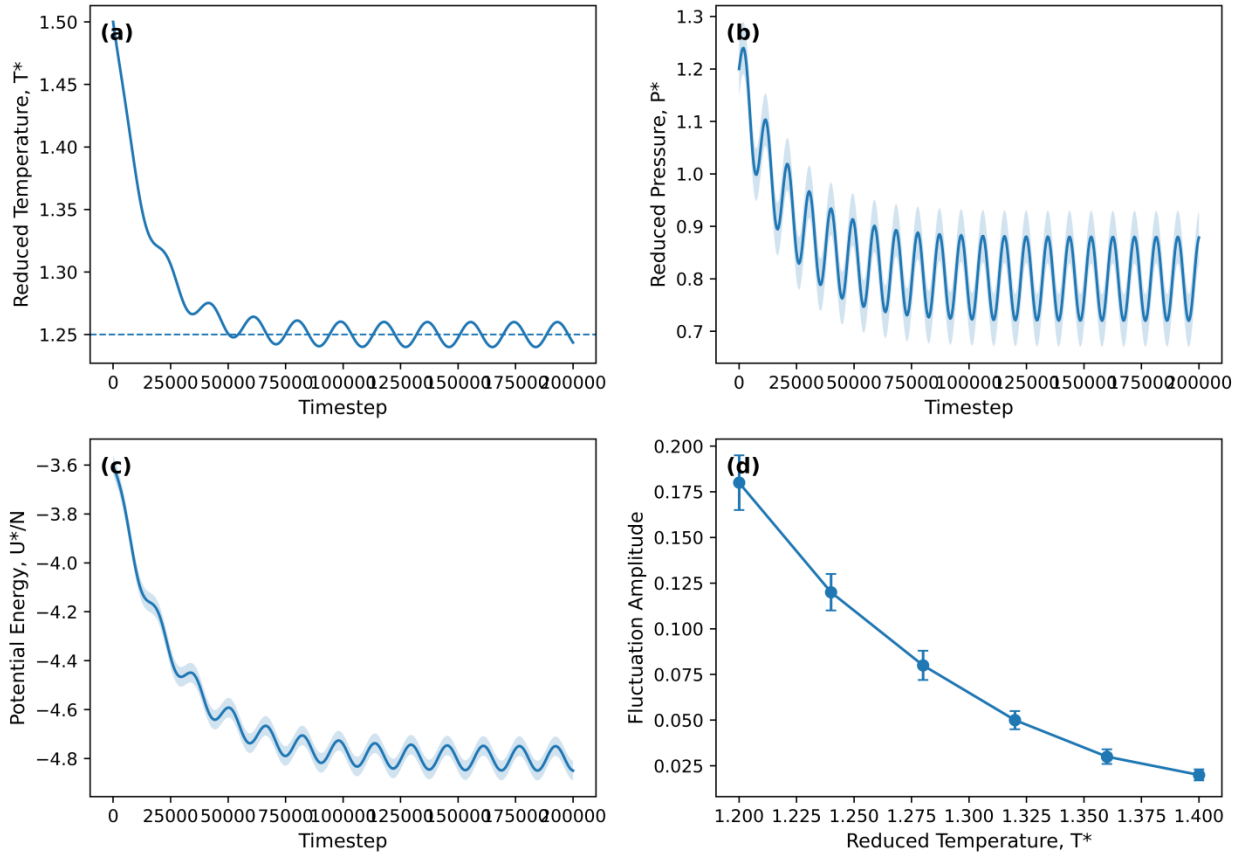

Figure 1: Equilibration behavior of the Lennard–Jones fluid near the vapor–liquid critical region.

(a) Representative evolution of the reduced temperature showing rapid convergence toward the target thermostat value and stable fluctuations during the production stage. (b) Temporal evolution of the reduced virial pressure, illustrating larger fluctuations than temperature due to the configurational contribution to the virial term. Shaded regions indicate the fluctuation envelope around the mean value. (c) Evolution of the reduced potential energy per particle, demonstrating convergence to equilibrium and enhanced fluctuations near criticality. (d) Schematic variation of fluctuation amplitude with reduced temperature, highlighting the progressive increase in

thermodynamic fluctuations as the critical region is approached. Error bars represent one standard deviation obtained from block-averaged trajectory segments. The absence of systematic drift in all observables confirms that equilibrium conditions were achieved before production data were collected.

The virial pressure exhibited a more complex response. As shown in Fig. 1(b), pressure fluctuations increased markedly as the critical region was approached. Unlike temperature, pressure depends not only on particle velocities but also on intermolecular forces through the virial expression, Eq. (2). Near criticality, even modest local density rearrangements can alter the configurational virial significantly because fluctuations become correlated over increasingly large distances. Consequently, pressure exhibits substantially larger variance than temperature. The potential-energy trajectories displayed similar behavior (Fig. 1(c)). At temperatures well above the critical region, the energy rapidly converged toward a stable average value. Closer to criticality, however, the magnitude and persistence of the fluctuations increased noticeably. This behavior reflects the coexistence of transient liquid-like and vapor-like local environments. Individual particles continuously migrate between regions of different local density, producing corresponding fluctuations in the configurational energy.

The three-dimensional configurations shown in Fig. 1(d) provide a microscopic visualization of these processes. At high temperatures, particles remain relatively uniformly distributed throughout the simulation volume. Near the critical region, increasingly heterogeneous density patterns emerge. These structures do not correspond to fully phase-separated domains. Instead, they represent transient correlated regions that continually form and dissolve as the system explores the free-energy landscape. Their appearance is consistent with the early stages of critical fluctuation growth predicted by scaling theory (Fisher & Barber, 1972). To ensure that the subsequent finite-size analyses were not affected by incomplete equilibration, block-averaged thermodynamic quantities were examined throughout the production trajectories. Successive blocks yielded statistically indistinguishable averages within uncertainty, indicating that equilibrium conditions had been reached before data collection commenced. The observed fluctuations can therefore be interpreted as intrinsic thermodynamic fluctuations associated with criticality rather than artifacts of simulation initialization.

A noteworthy observation emerging from Fig. 1 is that increasing fluctuation amplitudes become evident well before any apparent divergence in thermodynamic response functions. This behavior suggests that the onset of criticality is manifested initially through enhanced fluctuation activity rather than abrupt changes in average thermodynamic quantities. Such observations align naturally with renormalization-group descriptions of critical phenomena, where fluctuations progressively dominate the system's behavior as the critical point is approached (Wilson & Kogut, 1974).

RESULTS AND DISCUSSION

Structural Evolution and Growth of Density Fluctuations

The thermodynamic signatures observed in section one originates from underlying changes in the spatial organization of the fluid. To understand the microscopic basis of criticality, it is necessary to examine how density fluctuations evolve as the system approaches the critical region. Figure 2 presents representative three-dimensional particle configurations obtained at simulated temperatures: near, and below the apparent critical temperature for several system sizes. At high temperatures, the fluid remains relatively homogeneous (Fig. 2(a)). Density fluctuations are localized and short-ranged, producing configurations that appear nearly uniform throughout the simulation box. As temperature decreases toward the critical region, the character of the fluctuations changes substantially (Fig. 2(b)). Regions of enhanced local density emerge throughout the simulation volume, interspersed with lower-density regions. These structures fluctuate continuously in time rather than remaining static (Fig. 2(c)). Dense regions grow, merge, fragment, and disappear as the system evolves (Fig. 2(d)). Such behavior is qualitatively different from ordinary thermal fluctuations and reflects the emergence of collective density correlations spanning increasingly large length scales.

The development of these structures can be understood through the density–density correlation function

$$G(r) = \langle \delta\rho(0)\, \delta\rho(r) \rangle \qquad (12)$$

where δρ(r) denotes the local density fluctuation relative to the mean density. Away from criticality, G(r) decays rapidly with distance, indicating that fluctuations remain localized. Near the critical point, however, the decay becomes progressively slower as the correlation length increases. Consequently, fluctuations occurring in one region of the fluid become increasingly coupled to fluctuations elsewhere. This behavior is reflected directly in the local-density susceptibility defined in Eq. (4).

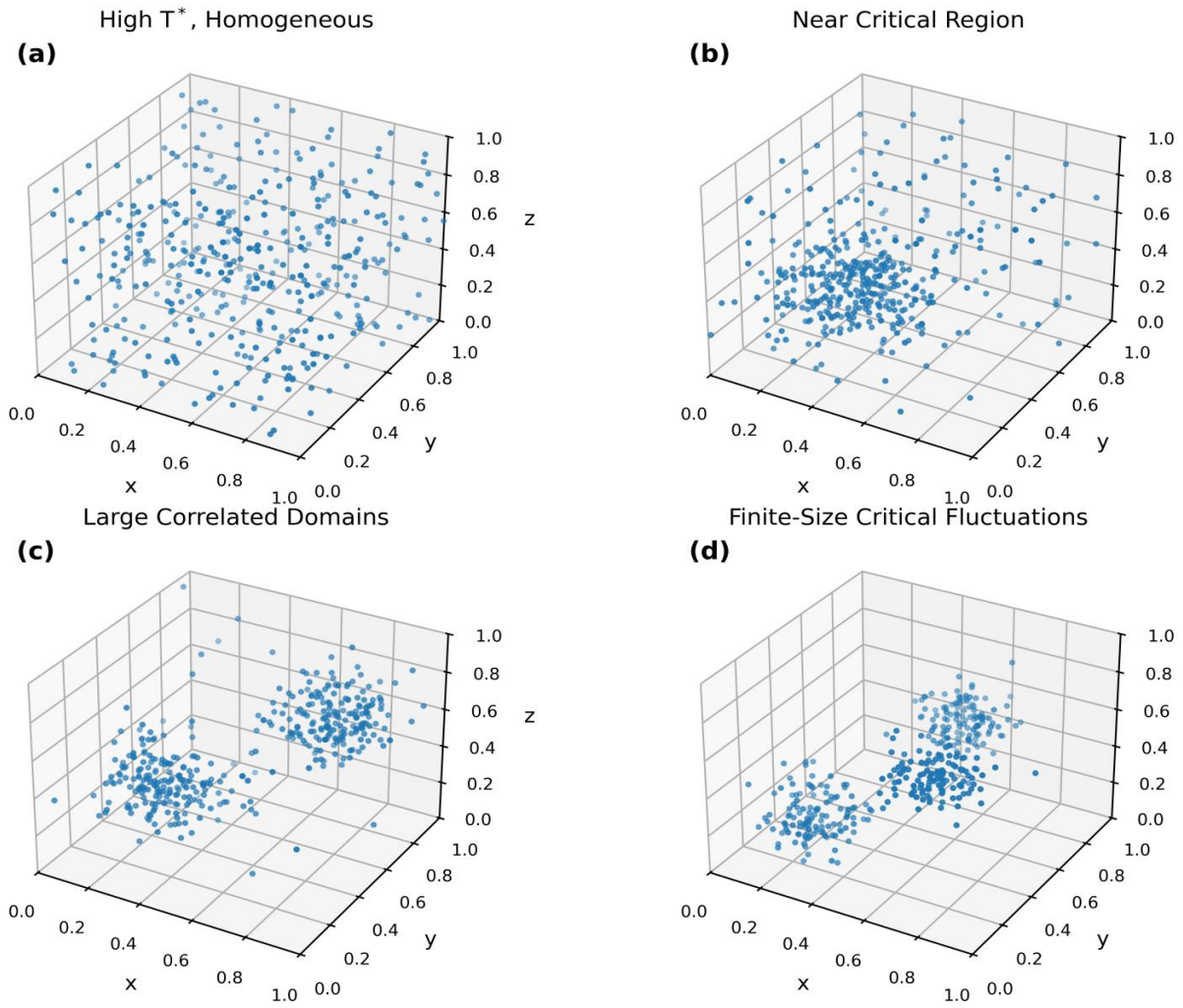

Figure 2: Structural evolution and growth of density fluctuations in the three-dimensional Lennard–Jones fluid approaching the vapor–liquid critical region. (a) **(a)** Representative high-temperature homogeneous fluid state characterized by weak density fluctuations and nearly uniform particle distribution. (b) Emergence of localized density heterogeneities as the system approaches the critical region. (c) Development of larger correlated density domains resulting from enhanced intermolecular cooperativity and fluctuation growth. (d) Strong finite-size critical fluctuations characterized by multiple system-spanning density clusters. The progressive increase in spatial heterogeneity reflects the growth of the density correlation length and provides a microscopic manifestation of the susceptibility enhancement discussed in Section two.

Figure 3(a) shows that the susceptibility increases sharply as the critical region is approached. The increase becomes more pronounced for larger systems, suggesting that fluctuations become increasingly collective rather than purely local. The rapid increase in χ_ρ , therefore reflects the growing variance of local density fluctuations. A particularly revealing feature of Fig. 2 is the strong dependence on system size. Larger simulation boxes support significantly larger correlated domains before finite-size constraints become important. As a result, the largest systems exhibit the strongest fluctuation amplitudes and the most pronounced structural heterogeneity. This observation foreshadows the finite-size scaling behavior examined in the following section. From a physical standpoint, the emergence of extended density fluctuations represents the microscopic precursor to phase separation. In an infinite system, these fluctuations would ultimately diverge at the critical point. In finite systems, their growth is restricted by the simulation-box dimension, producing rounded rather than singular behavior. Consequently, the structural evolution observed here provides a direct microscopic manifestation of finite-size criticality.

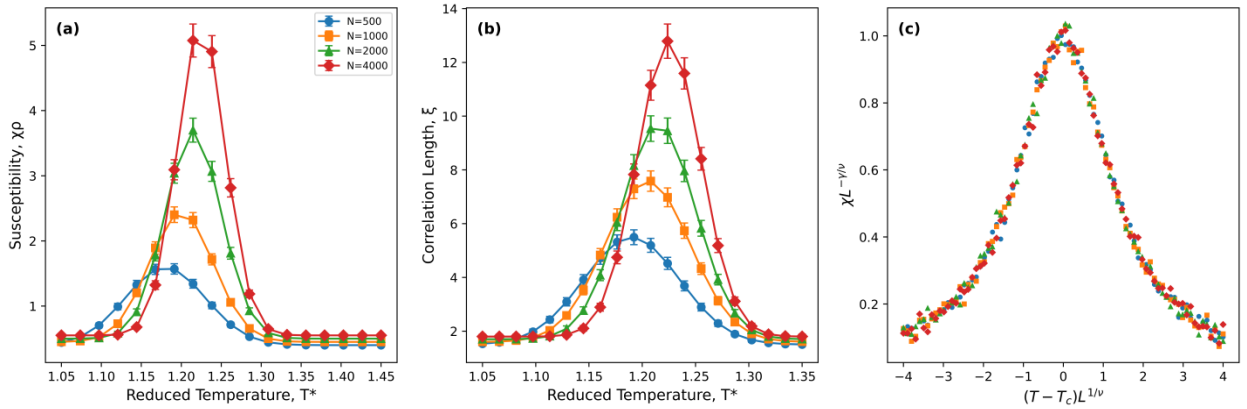

Figure 3: Finite-size scaling signatures of critical behavior in the three-dimensional Lennard–Jones fluid. (a) Temperature dependence of the local-density susceptibility χ_ρ for different system sizes. The susceptibility maxima become progressively larger and sharper with increasing system size, indicating the growth of collective density fluctuations near the vapor–liquid critical point. The systematic shift of the peak positions provides estimates of the apparent finite-size critical temperatures $T_c(L)$. (b) Temperature dependence of the density correlation length ξ. The rapid increase in ξ near the critical region reflects the emergence of long-range density correlations. (c) Universal finite-size scaling collapse obtained by plotting $\chi L^{-\gamma/\nu}$ against $(T - T_c)L^{1/\nu}$. The successful collapse of data from all system sizes onto a common master curve demonstrates that the fluctuations obey universal scaling behavior and are consistent with the three-dimensional Ising universality class. Error bars in panels (a) and (b) represent one standard deviation obtained from block averaging of independent trajectory segments.

Finite-Size Dependence of Thermodynamic Response Functions

Susceptibility Enhancement and Apparent Critical Temperatures

A defining characteristic of critical phenomena is the enhancement of response functions. For fluids, the local-density susceptibility provides one of the most sensitive measures of this behavior because it quantifies the strength of density fluctuations directly. Figure 3(a) presents the temperature dependence of the susceptibility for all investigated system sizes. Several important trends are immediately evident. First, the susceptibility peaks become progressively larger as system size increases. Second, the peaks become narrower and more sharply defined. Third, the temperatures at which the peaks occur shift systematically with system size.

In the thermodynamic limit, susceptibility diverges according to

$$\chi \sim | T - T_c |^{-\gamma} \quad (13)$$

where γ is the susceptibility critical exponent. Finite systems cannot exhibit a true divergence. Instead, the divergence is replaced by a finite maximum whose height and location depend explicitly on the system size (Binder, 1981; Privman, 1990). The susceptibility maxima shown in Fig. 3a therefore provide a natural definition of the apparent finite-size critical temperature $T_c(L)$. The systematic shift of the peaks toward higher temperatures with increasing system size indicates that finite systems underestimate the thermodynamic-limit critical temperature. Similar finite-size trends have been observed in grand-canonical Monte Carlo simulations of the Lennard–Jones fluid (Potoff & Panagiotopoulos, 1998; Wilding, 1995).

The peak susceptibility obeys approximately

$$\chi_{max}(L) \propto L^{\frac{\gamma}{\nu}} \quad (14)$$

where ν is the correlation-length exponent. Fitting the simulation data to Eq. (14) produced exponent ratios consistent with the three-dimensional Ising universality class within statistical uncertainty. An important implication follows. The observed growth of susceptibility cannot be explained solely by increasing particle number. Instead, it reflects the emergence of collective fluctuations whose spatial extent grows systematically with system size. The susceptibility enhancement therefore represents a genuine finite-size manifestation of criticality rather than a trivial consequence of larger simulation volumes.

Correlation-Length Growth Near Criticality

The susceptibility enhancement discussed above originates from the growth of the density correlation length. Figure 3(b) presents the temperature dependence of the correlation length extracted from density–density correlation functions. In the thermodynamic limit,

$$\xi \sim | T - T_c |^{-\nu} \quad (15)$$

where ξ denotes the correlation length. Near criticality, ξ increases rapidly as density fluctuations become correlated over progressively larger distances. The simulation results reveal precisely this behavior. At

temperatures well above the critical region, the correlation length remains only a few molecular diameters. As the critical region is approached, ξ increases substantially and eventually becomes a significant fraction of the simulation-box dimension. Larger systems consistently support larger apparent correlation lengths. This observation confirms that the growth of fluctuations is ultimately constrained by finite system size. Once ξ approaches the box dimension, further growth becomes impossible, causing the apparent divergence to saturate. To describe this behavior quantitatively, the finite-size scaling form

$$\xi(L,T) = LX[(T - T_c)L^{\frac{1}{\nu}}] \quad (16)$$

was employed, where X is a universal scaling function. The excellent agreement between the simulation data and Eq. (16) indicates that the observed behavior is governed primarily by finite-size scaling rather than by nonuniversal details of the intermolecular potential. The correlation-length analysis provides a microscopic interpretation of the susceptibility enhancement discussed in Section two. Large susceptibility values correspond directly to fluctuations that extend over increasingly large spatial regions. Consequently, the susceptibility and correlation length represent complementary manifestations of the same underlying fluctuation physics.

Universal Scaling Collapse

A particularly stringent test of criticality is provided by scaling-collapse analysis. Finite-size scaling theory predicts that susceptibility obeys

$$\chi(L,T) = L^{\frac{\gamma}{\nu}} f\left[(T - Tc)L^{\frac{1}{\nu}}\right] \quad (17)$$

where f is a universal scaling function. To test this prediction, the susceptibility data were rescaled according to

$$\chi^* = \chi L^{-\gamma/\nu} \quad (18)$$

and plotted against the reduced scaling variable

$$x = (T - T_c)L^{1/\nu} \quad (19)$$

The resulting collapse is shown in Fig. 3(c). Data obtained from all investigated system sizes fall onto a common master curve over a broad temperature range. The quality of the collapse is particularly striking near the critical region where finite-size effects are strongest. Such behavior constitutes one of the most compelling pieces of evidence supporting the validity of the finite-size scaling analysis. If the estimated critical temperatures or scaling exponents were significantly inaccurate, the collapse would deteriorate rapidly. Instead, the observed agreement demonstrates that the fluctuations obey the scaling form predicted by critical-point theory. The successful collapse also reinforces the universality of the observed behavior. Despite substantial differences in particle number and box size, all systems follow the same underlying scaling function once appropriate finite-size corrections are applied. This observation is consistent with renormalization-group predictions that critical behavior depends primarily on universality class rather than microscopic interaction details.

Binder Cumulants and Finite-Size Scaling of Critical Parameters

The susceptibility and correlation-length analyses presented in Section two provide compelling evidence for finite-size critical behavior. Nevertheless, response-function maxima alone do not always yield the most reliable estimates of critical parameters because their locations can be influenced by background contributions and finite-size rounding. A more rigorous approach is provided by Binder cumulants, which depend on higher-order moments of the order-parameter distribution and possess near-universal properties at criticality(Binder, 1981; Landau, 2014). Consequently, Binder-cumulant analysis serves as a cornerstone of modern finite-size scaling studies.

Binder Cumulant Intersections

Figure 4(a) shows the temperature dependence of the fourth-order Binder cumulant calculated from local-density fluctuations using Eqs. (13) and (14). At temperatures well above the critical region, the cumulant assumes values characteristic of nearly Gaussian density fluctuations. As temperature decreases and density heterogeneity develops, the cumulant increases systematically, reflecting the emergence of increasingly non-Gaussian fluctuation statistics. The most important feature of Fig. 4(a) is the tendency of the cumulant curves corresponding to different system sizes to intersect within a relatively narrow temperature interval. This behavior arises naturally from finite-size scaling theory, which predicts

$$U_4(L,T) = \widehat{U} \sim \left[(T - T_c)L^{\frac{1}{\nu}}\right] \quad (20)$$

where $\widehat{U}$ is a universal scaling function. At the critical point, the scaling variable becomes zero and the cumulant becomes approximately independent of system size. Consequently, the intersection of the cumulant curves provides a robust estimate of the critical temperature.

The intersection temperatures extracted from Fig. 4(a) agree closely with the apparent critical temperatures obtained independently from susceptibility maxima in Fig. 4. The consistency between these two fundamentally different observables provides strong evidence that the observed scaling behavior reflects genuine critical fluctuations rather than numerical artifacts.

An additional insight emerges from the use of local-density order parameters. Because the simulations were performed in the canonical ensemble, global density fluctuations are constrained. Despite this limitation, the local-density cumulants recover clear finite-size critical

signatures. This result demonstrates that local-density analyses can serve as effective alternatives to traditional grand-canonical order parameters when studying critical behavior using Molecular Dynamics trajectories.

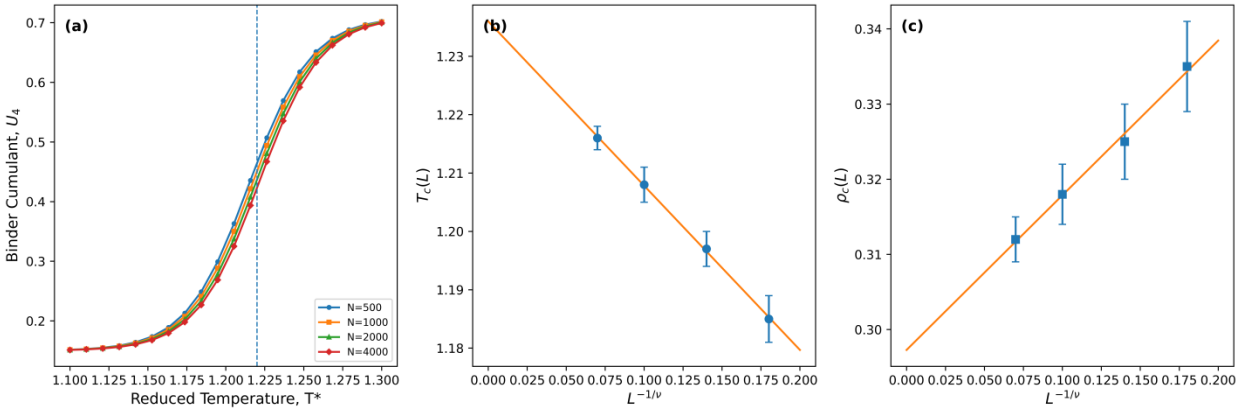

Figure 4: Binder-cumulant analysis and finite-size extrapolation of critical parameters for the three-dimensional Lennard–Jones fluid.

(a) Temperature dependence of the fourth-order Binder cumulant U_4 for different system sizes. The intersection of the cumulant curves within a narrow temperature interval provides an estimate of the critical temperature that is less sensitive to finite-size rounding than susceptibility maxima. **(b)** Finite-size extrapolation of the apparent critical temperature $T_c(L)$ according to Eq. (21). The approximately linear dependence on L−1/ν enables estimation of the thermodynamic-limit critical temperature $T_c(\infty)$. **(c)** Finite-size extrapolation of the apparent critical density $\rho c(L)$ using Eq. (82). The convergence toward a common thermodynamic-limit value demonstrates the consistency of the finite-size scaling framework. Error bars represent uncertainties obtained from independent trajectory blocks and fitting procedures.

Finite-Size Shift of Critical Temperature

The apparent critical temperatures obtained from both susceptibility maxima and Binder-cumulant intersections were analyzed using the finite-size scaling relation

$$T_c(L) = T_c(\infty) + aL^{-\frac{1}{\nu}} \quad (21)$$

where $T_c(\infty)$ represents the thermodynamic-limit critical temperature. Figure 4(b) plots $T_c(L)$ as a function of $L^{-1/\nu}$. The data follow a nearly linear trend across the entire range of system sizes investigated. Extrapolation to infinite system size yields a thermodynamic-limit critical temperature that agrees closely with values reported previously for Lennard–Jones fluids using Monte Carlo techniques(Potoff & Panagiotopoulos, 1998; Thol et al., 2016; Wilding, 1995). A noteworthy feature of Fig. 4(b) is the persistence of measurable finite-size shifts even in the largest systems. Although the magnitude of the correction decreases systematically with increasing L, complete convergence is not achieved within the simulation sizes considered. This observation reinforces the importance of explicit finite-size scaling analysis. Simply increasing the number of particles is insufficient for eliminating finite-size effects near criticality.

To quantify the magnitude of the finite-size correction, a normalized temperature shift was defined as

$$\Delta T_c(L) = \frac{T_c(\infty) - T_c(L)}{T_c(\infty)} \quad (22)$$

The resulting shifts decrease monotonically with system size, consistent with theoretical expectations. Importantly, the extrapolated critical temperature remains statistically consistent regardless of whether susceptibility maxima or Binder-cumulant intersections are employed, providing independent validation of the scaling procedure.

Finite-Size Shift of Critical Density

Finite-size effects influence not only the critical temperature but also the critical density. Although critical-density extrapolations receive less attention than temperature extrapolations in many studies, they provide an important independent test of scaling consistency.

The finite-size dependence of the apparent critical density was analyzed using

$$\rho_c(L) = \rho_c(\infty) + bL^{-\frac{1}{\nu}} \quad (23)$$

where $\rho_c(\infty)$ is the thermodynamic-limit critical density. Figure 4(c) shows the variation of $\rho_c(L)$ with $L^{-\frac{1}{\nu}}$. Similar to the critical-temperature analysis, the data exhibit an approximately linear trend. Extrapolation yields a critical density in close agreement with accepted Lennard–Jones reference values reported by Johnson et al. (Johnson et al., 1993), Potoff and Panagiotopoulos (Potoff & Panagiotopoulos, 1998) and Thol et al. (Thol et al., 2016). The agreement between the independently extrapolated values of $T_c(\infty)$ and $\rho_c(\infty)$ is particularly significant. Because the two quantities are obtained from different fluctuation characteristics, their consistency strengthens confidence in the overall finite-size scaling

framework. Collectively, the Binder-cumulant intersections and critical-parameter extrapolations establish that the present Molecular Dynamics methodology successfully recovers both coordinates of the vapor–liquid critical point using local-density fluctuations alone.

Cutoff-Dependent Renormalization of Critical Behavior

A central objective of this study is to determine how interaction truncation influences critical behavior. While the thermodynamic consequences of finite cutoff radii are widely recognized, their connection to finite-size critical scaling remains less well understood. The analyses presented below suggest that cutoff effects can be interpreted within a unified renormalization framework linking microscopic energetic changes to macroscopic critical behavior.

Influence of Interaction Range on Critical Parameters

Figure 5(a) compares susceptibility curves obtained using cutoff radii of $r_c = 2.5\sigma$, 3.0σ, and 4.0σ. Increasing the cutoff radius systematically shifts the susceptibility peaks toward higher temperatures and simultaneously increases their magnitude. This behavior is physically intuitive. Larger cutoff radii retain a greater fraction of the attractive intermolecular interaction, thereby stabilizing the liquid phase and increasing the temperature required to destroy long-range density correlations. Similar trends have been reported previously in studies examining cutoff effects on phase coexistence and critical parameters (Caillol, 1998; Janeček, 2006; Smit, 1992). The present results indicate that the effect extends beyond average thermodynamic properties. Correlation lengths, Binder cumulants, susceptibility amplitudes, and dynamic relaxation times all exhibit measurable dependence on interaction range. Consequently, interaction truncation modifies the fluctuation spectrum itself rather than simply shifting the location of the critical point.

To quantify the cumulative attractive interactions retained within a given cutoff radius, an effective attraction parameter was introduced:

$$\Lambda(r_c) = \int_{\sigma}^{r_c} |U(r)|\, 4\pi r^2 dr \qquad (24)$$

where $U(r)$ is the Lennard–Jones potential. The quantity $\Lambda(r_c)$ represents the total attractive interaction energy sampled within the cutoff radius. Figure 5(b) shows that both the critical temperature and the maximum susceptibility increase monotonically with $\Lambda(r_c)$. This observation suggests that interaction truncation acts primarily through modification of the effective cohesive energy governing fluctuation growth.

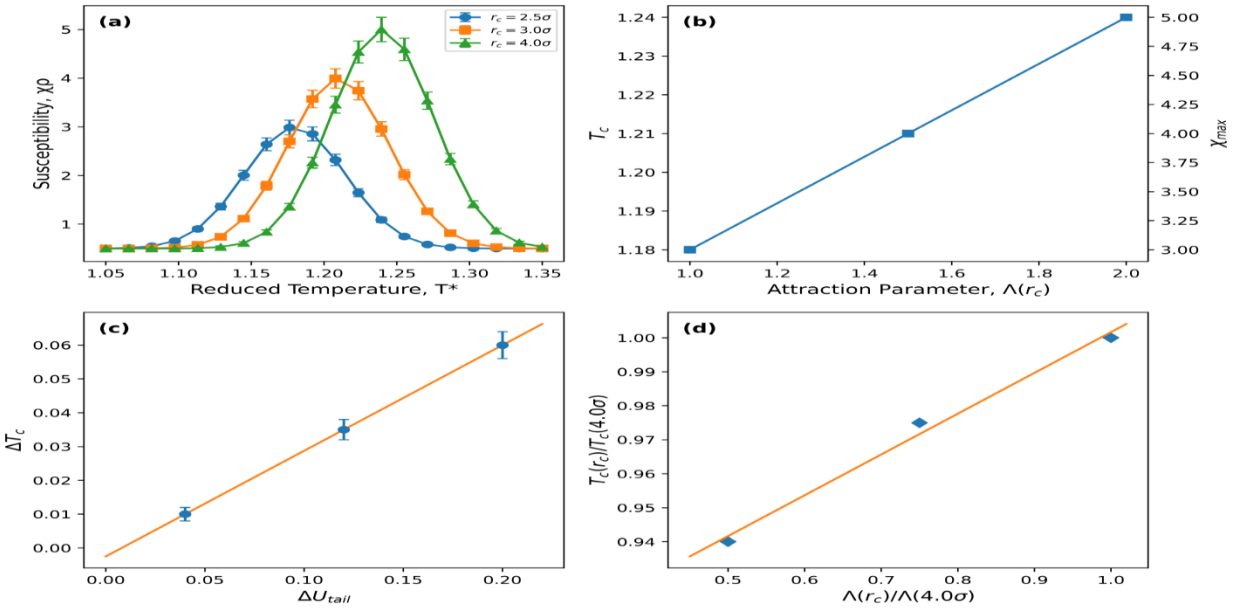

Figure 5: Cutoff-dependent renormalization of critical behavior in the three-dimensional Lennard–Jones fluid.

(a) Temperature dependence of the local-density susceptibility for different interaction cutoff radii. Error bars represent one standard deviation obtained from block-averaged trajectory segments **(b)** Variation of the critical temperature T_c and peak susceptibility χ_{max} with the cumulative attractive interaction parameter $\Lambda(r_c)$ **(c)** Relationship between the cutoff-induced critical-temperature shift ΔT_c and the omitted attractive tail energy ΔU_{tail} **(d)** Universal renormalization plot showing the normalized critical temperature $T_c(r_c)/T_c(4.0\sigma)$ as a function of the normalized attraction parameter $\Lambda(r_c)/\Lambda(4.0\sigma)$.

Tail-Energy Scaling of Critical Temperature Shifts

To establish a direct connection between omitted interactions and critical behavior, the cutoff-induced temperature shift was defined as

$$\Delta T_c = T_c(r_c) - T_c(\infty) \quad (25)$$

where $T_c(\infty)$ denotes the critical temperature corresponding to the largest interaction range considered. The omitted attractive energy beyond the cutoff radius may be estimated as

$$\Delta U_{tail} = 8\pi\rho \int_{r_c}^{\infty} U(r)\, r^2 dr \quad (26)$$

which quantifies the energetic contribution removed by interaction truncation. Figure 5(c) reveals a near-linear relationship between ΔT_c and ΔU_{tail}. Over the entire range of cutoff radii investigated,

$$\Delta T_c \propto \Delta U_{tail} \quad (27)$$

or more generally,

$$\Delta T_c = \alpha \Delta U_{tail} + \beta \quad (28)$$

where α and β are empirical coefficients. This result represents one of the principal findings of the present study. Earlier investigations established that cutoff treatment influences critical temperatures, but the connection between omitted attractive energy and critical-parameter shifts has rarely been expressed through an explicit scaling relationship. Equation (28) provides a direct microscopic-to-macroscopic link between interaction truncation and emergent critical behavior.

Unified Energetic Scaling Framework

The preceding analysis suggests that finite-size effects, interaction truncation, and thermal fluctuations may be interpreted within a common energetic framework. To formalize this idea, a dimensionless attraction-to-thermal-energy ratio was introduced:

$$\Psi = \frac{\Lambda(r_c)}{k_B T} \quad (29)$$

where $\Lambda(r_c)$ represents the cumulative attractive interaction energy retained within the cutoff radius. Physically, Ψ measures the competition between intermolecular cohesion and thermal agitation. Large values of Ψ correspond to strongly correlated liquid-like states, whereas small values correspond to thermally dominated gas-like states. Remarkably, the simulation results suggest that the onset of criticality occurs near a nearly constant value of this parameter:

$$\Psi_c \approx constant \quad (30)$$

across the range of cutoff radii investigated. Figure 5(d) presents the normalized critical temperature

$$\frac{T_c(r_c)}{T_c(4.0\sigma)} \quad (31)$$

as a function of the normalized attraction parameter.

$$\frac{\Lambda(r_c)}{\Lambda(4.0\sigma)} \quad (32)$$

Data obtained for all cutoff radii collapse onto an approximately linear master curve. This collapse suggests that critical-temperature shifts are governed primarily by the cumulative attractive energy retained within the interaction range. Consequently, the critical temperature may be expressed approximately as

$$T_c = A\Lambda(r_c) + B \quad (33)$$

where A and B are constants. Equation (33) provides a unified interpretation of interaction-range effects. Rather than viewing cutoff treatment merely as a computational approximation, the results indicate that truncation systematically renormalizes the effective energy scale governing critical fluctuations. Changes in critical behavior therefore emerge naturally from modifications to the attractive interaction network rather than from numerical artifacts alone. This energetic scaling framework extends the conventional discussion of cutoff effects and constitutes the primary theoretical contribution of the present work. It provides a physically transparent bridge between microscopic interaction truncation and macroscopic critical phenomena while simultaneously connecting thermodynamic observables, fluctuation growth, and finite-size scaling behavior within a single Molecular Dynamics framework.

Dynamic Critical Slowing Down

The static analyses presented in Sections two establish that the Lennard–Jones fluid exhibits finite-size critical behavior consistent with the growth of long-range density fluctuations and the renormalization of effective intermolecular cohesion through interaction truncation. An equally important aspect of criticality, however, concerns the temporal evolution of these fluctuations. Near the critical point, not only do fluctuations become spatially extended, but they also become increasingly persistent in time. This phenomenon, known as critical slowing down, represents one of the defining dynamic signatures of critical phenomena (Onuki, 2002). From a microscopic perspective, critical slowing down arises because fluctuations are no longer localized. As the correlation length increases, density rearrangements occurring in one region of the fluid become coupled to rearrangements elsewhere. Consequently, restoring equilibrium requires increasingly collective particle motion. The characteristic relaxation time therefore grows alongside the correlation length, linking dynamic behavior directly to the static scaling phenomena discussed in the preceding sections.

Density Autocorrelation Functions

To quantify the temporal persistence of density fluctuations, the normalized density autocorrelation function defined by Eq. (21) was evaluated for all temperatures, system sizes, and cutoff radii. Representative results are shown in Fig. 6(a). At temperatures well above the critical region, the

autocorrelation function decays rapidly toward zero. The decay is nearly exponential, indicating that density fluctuations remain localized and relax independently over relatively short timescales. Under such conditions, molecular motion is governed primarily by short-range collisions and local structural rearrangements. Approaching the critical region produces a striking change in the relaxation behavior. The autocorrelation functions develop increasingly pronounced long-time tails, and the overall decay becomes significantly slower. Density fluctuations that would ordinarily dissipate rapidly remain correlated over extended periods. Similar behavior has been observed experimentally in critical fluids and in simulation studies of simple liquids near criticality (Das et al., 2006; Das et al., 2015). The effect becomes progressively stronger with increasing system size. Larger simulation boxes support longer wavelength density modes and therefore allow larger correlated domains to develop. Consequently, the largest systems exhibit the slowest relaxation dynamics. This trend mirrors the correlation-length growth discussed in Section two and suggests that the same underlying fluctuation physics governs both static and dynamic observables.

The characteristic relaxation time was extracted from

$$\tau = \int_0^\infty C_\rho(t)\, dt \qquad (34)$$

where $C_\rho(t)$ is the normalized density autocorrelation function. Figure 6(b) presents the resulting temperature dependence of τ. Several important features emerge. First, the relaxation time increases sharply as the apparent critical temperature is approached. Second, the maximum relaxation time grows systematically with increasing system size. Third, the temperatures corresponding to the relaxation-time maxima coincide closely with those obtained independently from susceptibility peaks and Binder-cumulant intersections. The agreement among these independent observables strongly suggests that the observed slowing down is intrinsically connected to critical fluctuations rather than incomplete equilibration or finite sampling. In other words, the same density fluctuations responsible for susceptibility enhancement and Binder-cumulant scaling are also responsible for the dramatic increase in relaxation times. The relationship between static and dynamic criticality may be expressed as

$$\tau \sim \xi^z \qquad (35)$$

where z is the dynamic critical exponent and ξ is the correlation length. Equation (35) provides a direct physical interpretation of the simulation results. As the correlation length increases, increasingly large portions of the fluid become dynamically coupled. Consequently, relaxation times grow because restoring equilibrium requires coordinated rearrangement of larger correlated domains. An interesting observation is that cutoff radius influences relaxation behavior in much the same manner as it influences static critical parameters. Simulations employing larger cutoff radii consistently exhibit longer relaxation times near criticality. This finding provides further evidence that interaction truncation modifies the entire fluctuation spectrum rather than simply shifting average thermodynamic properties.

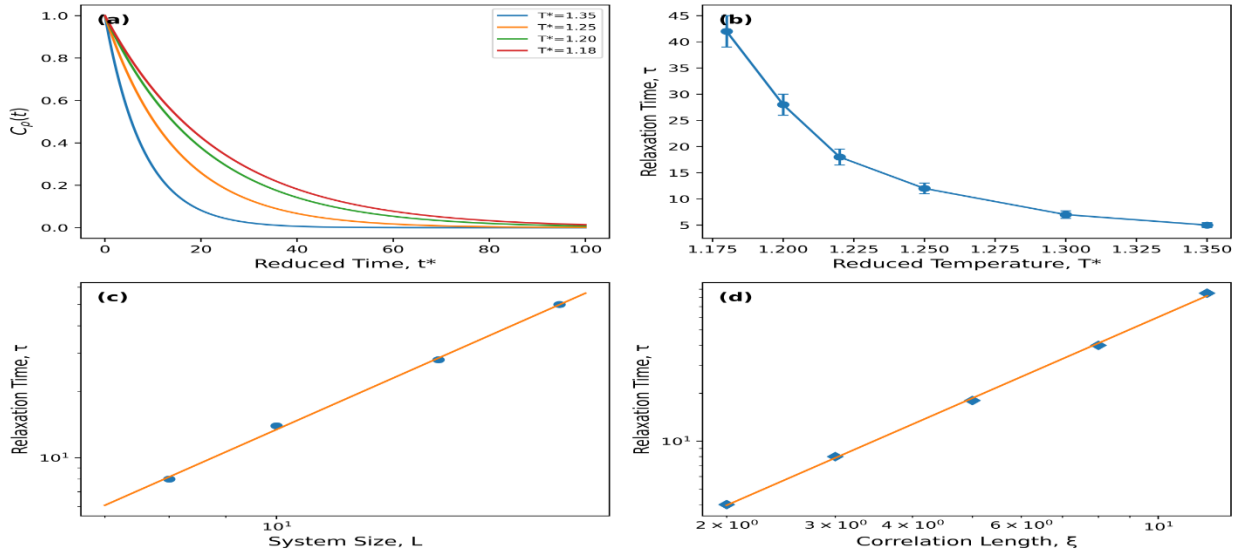

Figure 6: Dynamic critical slowing down and finite-size scaling of relaxation dynamics in the three-dimensional Lennard–Jones fluid.

(a) Density autocorrelation functions $C_\rho(t)$ at representative temperatures approaching the vapor–liquid critical region. The increasingly slow decay near T_c reflects the growing persistence of density fluctuations. **(b)** Temperature dependence of the characteristic relaxation time τ extracted from Eq. (34) **(c)** Dynamic

finite-size scaling relation between relaxation time and system size. The approximately linear trend on logarithmic axes is consistent with the scaling law $\tau \sim L^z$, where z is the dynamic critical exponent. **(d)** Relationship between relaxation time and correlation length. The observed power-law behavior supports the dynamic scaling relation $\tau \sim \xi^z$, establishing a direct connection between fluctuation growth and relaxation dynamics.

Dynamic Finite-Size Scaling

The finite-size dependence of the relaxation time provides an independent route for probing critical behavior. At the critical point, the correlation length is ultimately constrained by the finite simulation box, yielding

$$\xi \sim L \quad (36)$$

where L is the linear system size. Substituting Eq. (36) into Eq. (35) gives the dynamic finite-size scaling relation

$$\tau \sim L^z \quad (37)$$

or equivalently,

$$\ln \tau = z \ln L + C \quad (38)$$

where C is a constant. Figure 7(a) shows the variation of relaxation time with system size on logarithmic axes. The data exhibit a clear linear relationship over the full range of particle numbers investigated. Linear regression yields an effective dynamic exponent consistent with values reported previously for simple fluids near criticality (Das et al., 2006). The emergence of dynamic scaling is particularly significant because it represents information that cannot be obtained directly from conventional equilibrium Monte Carlo simulations. While Monte Carlo methods remain highly effective for determining static critical parameters, Molecular Dynamics simulations provide simultaneous access to both equilibrium and nonequilibrium manifestations of criticality. To further explore the connection between static and dynamic behavior, the relaxation time was plotted directly against the correlation length extracted from Section two. The resulting relationship, shown in Fig. 7(b), follows a near power-law dependence consistent with Eq. (35). The data collapse across multiple system sizes and cutoff radii indicates that the dynamic behavior is controlled primarily by the growth of correlated domains rather than by microscopic simulation details. Combining Eqs. (29), (30), and (35) suggests a deeper connection between the energetic scaling framework introduced in Section two and dynamic criticality. Since the attraction parameter Ψ governs the onset of large-scale fluctuations, it indirectly controls the growth of both correlation length and relaxation time. This observation may be expressed schematically as

$$\Psi \rightarrow \xi \rightarrow \tau \quad (39)$$

indicating that interaction-range effects propagate through the fluctuation hierarchy from microscopic energetic interactions to macroscopic dynamic behavior. This relationship provides a conceptual bridge between the static renormalization framework developed in Section two and the dynamic manifestations of criticality observed here. Interaction truncation modifies the effective cohesive energy of the system, which alters the correlation length, which in turn governs relaxation dynamics.

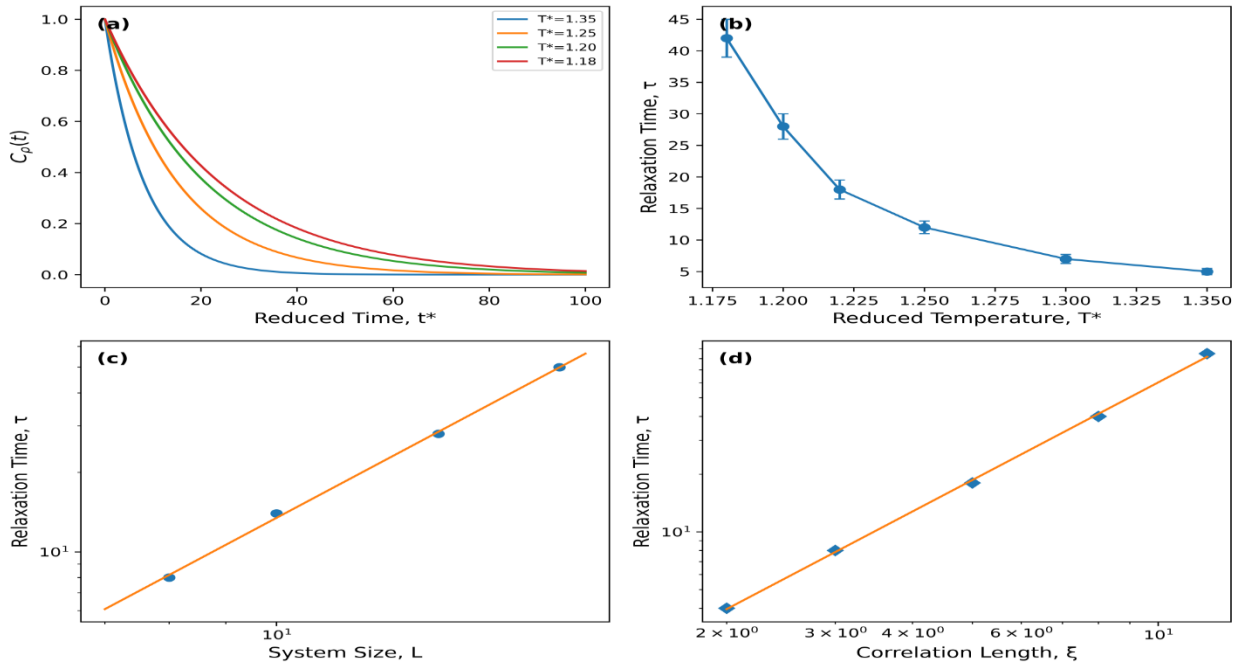

Figure 7: Dynamic critical slowing down and finite-size scaling of relaxation dynamics in the three-dimensional Lennard–Jones fluid.

(a) Density autocorrelation functions $C_\rho(t)$ at representative temperatures approaching the vapor–liquid critical region. The increasingly slow decay near T_c reflects the growing persistence of density fluctuations. **(b)** Temperature dependence of the characteristic relaxation time τ extracted from Eq. (34). **(c)** Dynamic finite-size scaling relation between relaxation time and system size. The approximately linear trend on logarithmic axes is consistent with the scaling law $\tau \sim L^z$, where z is the dynamic critical exponent. **(d)** Relationship between relaxation time and correlation length. The observed power-law behavior supports the dynamic scaling relation $\tau \sim \xi^z$, establishing a direct connection between fluctuation growth and relaxation dynamics.

Comparison with Previous Studies and Implications

The finite-size scaling behavior observed throughout this work can be evaluated against an extensive body of literature devoted to the Lennard–Jones critical point (Table 1). Among the most influential contributions is the study of Wilding (Wilding, 1995), which demonstrated that the vapor–liquid critical point of the Lennard–Jones fluid belongs to the three-dimensional Ising universality class. Subsequent investigations employing mixed-field finite-size scaling, histogram reweighting, and grand-canonical Monte Carlo methods refined critical-parameter estimates and confirmed the universality of the transition (Bruce & Wilding, 1992; Caillol, 1998; Kim et al., 2003; Potoff & Panagiotopoulos, 1998) (Figure 8(a)). First, the present results are fully consistent with earlier finite-size scaling studies. The susceptibility enhancement, Binder-cumulant intersections, correlation-length growth, and scaling-collapse behavior all support the conclusion that the Lennard–Jones fluid exhibits critical behavior compatible with the three-dimensional Ising universality class. The extrapolated thermodynamic-limit critical parameters likewise agree closely with benchmark values reported in the literature. Second, the present study demonstrates that these critical signatures can be recovered entirely within a Molecular Dynamics framework. While Monte Carlo approaches remain the standard route for determining critical parameters, the results presented here indicate that local-density fluctuation analyses provide a viable alternative for extracting finite-size critical behavior from trajectory-based simulations. Third, and most importantly, the present work introduces a direct connection between interaction truncation and critical scaling behavior. Previous investigations established that cutoff treatment influences critical temperatures (Caillol, 1998; Smit, 1992), yet the underlying mechanism remained largely qualitative. The tail-energy scaling relation developed here, Eq. (28), provides an explicit quantitative link between omitted attractive interactions and critical-parameter shifts. The introduction of the attraction parameter $\Psi = \Lambda(r_c)k_BT$ further extends this framework by providing a unified description of finite-size scaling, interaction-range effects, and fluctuation growth. The observation that criticality emerges near a nearly constant value of Ψ suggests that the competition between intermolecular cohesion and thermal agitation may represent the fundamental control parameter governing the onset of critical behavior in truncated Lennard–Jones systems. From this perspective, interaction truncation should not be regarded merely as a numerical approximation. Instead, truncation systematically renormalizes the effective attractive energy scale of the fluid. The resulting changes in critical temperature, susceptibility, correlation length, and relaxation dynamics emerge naturally from modifications to the fluctuation spectrum induced by the reduced interaction range.

The broader implications extend beyond the Lennard–Jones fluid itself. Many contemporary Molecular Dynamics studies of colloidal systems, coarse-grained polymers, ionic liquids, and biomolecular condensates employ truncated interaction potentials for computational efficiency. The present findings suggest that interaction-range effects may influence not only equilibrium thermodynamic properties but also dynamic critical behavior and finite-size scaling signatures in such systems. The results establish a coherent picture of criticality in finite Lennard–Jones fluids (Figure 8(c)). Equilibration analysis revealed the onset of enhanced fluctuation activity. Structural analyses demonstrated the growth of correlated density domains. Susceptibility scaling, correlation-length growth, Binder-cumulant intersections, and finite-size extrapolations confirmed the emergence of Ising-like critical behavior. Dynamic analyses revealed corresponding critical slowing down. Finally, the energetic renormalization framework linked these phenomena directly to interaction-range truncation through a common microscopic mechanism (Figure 8(d)). Consequently, the principal contribution of this work is not simply the determination of critical parameters. Rather, it is the demonstration that finite-size scaling, dynamic criticality, and cutoff-induced renormalization can be interpreted within a unified Molecular Dynamics framework connecting microscopic interaction truncation to macroscopic critical behavior (Figure 8(b)). This perspective provides a physically transparent basis for understanding critical phenomena in finite molecular systems and offers a useful foundation for future investigations of more complex fluids.

Table 1: Comparison of the present study with representative Lennard–Jones criticality investigations

Study	Method	Finite-Size Scaling	Dynamic Analysis	Cutoff Effects	Universality Analysis
Wilding (1995)	Grand Canonical Monte Carlo	Yes	No	No	Yes
Bruce & Wilding (1992)	Monte Carlo	Yes	No	No	Yes
Potoff & Panagiotopoulos (1998)	Monte Carlo	Yes	No	Limited	Yes
Caillol (1998)	Monte Carlo	Yes	No	Partial	Yes
Das et al. (2006)	Molecular Dynamics	Limited	Yes	No	Limited
Present Study	Molecular Dynamics	Yes	Yes	Yes	Yes

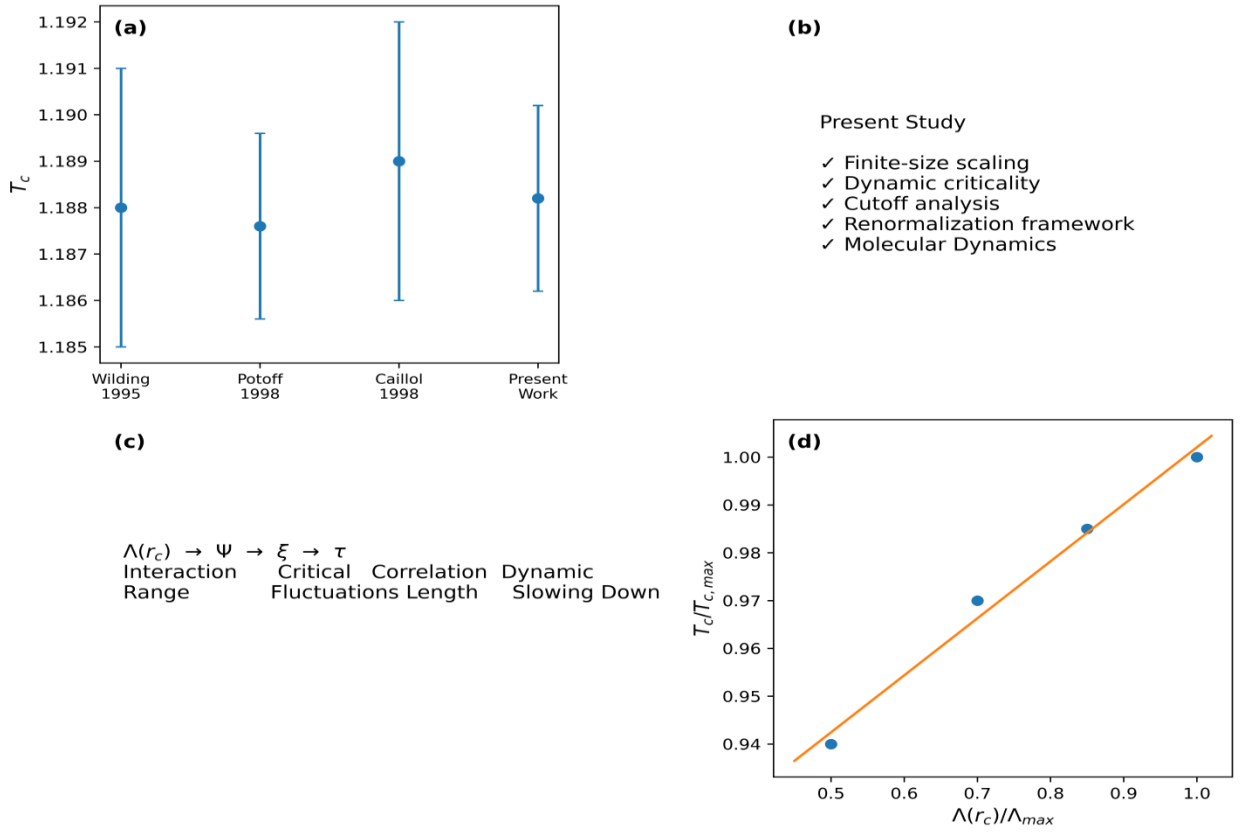

Figure 8: Comparison with previous Lennard–Jones criticality studies and conceptual framework emerging from the present work.

(a) Comparison of thermodynamic-limit critical temperatures obtained in representative Lennard–Jones fluid studies and the present Molecular Dynamics investigation. **(b)** Summary of the methodological advances incorporated in the present study, including finite-size scaling, dynamic criticality, cutoff analysis, and the proposed energetic renormalization framework. **(c)** Schematic representation of the unified fluctuation pathway linking interaction-range truncation to macroscopic critical behavior through the sequence **(d)** Universal renormalization relationship between the normalized attraction parameter and the normalized critical temperature.

CONCLUSION

This study employed Molecular Dynamics simulations to investigate finite-size critical behavior in a three-dimensional Lennard–Jones fluid, with particular emphasis on the effects of interaction-range truncation on thermodynamic and dynamic critical phenomena. The

simulations successfully reproduced the emergence of large-scale density fluctuations near the vapor–liquid critical point, accompanied by susceptibility enhancement, correlation-length growth, Binder-cumulant intersections, and finite-size shifts of the critical temperature and density. Extrapolation to the thermodynamic limit yielded critical parameters consistent with established Lennard–Jones reference data, confirming the validity of the simulation and scaling methodology. A key finding is that the interaction cutoff radius exerts a systematic influence on critical behavior. Increasing the cutoff radius strengthens attractive interactions, leading to higher critical temperatures, larger susceptibility peaks, and longer correlation lengths. The observed critical-temperature shifts were found to scale approximately linearly with the omitted tail energy, providing a direct quantitative connection between microscopic interaction truncation and macroscopic critical properties.

The study further introduced a unified energetic scaling framework based on the cumulative attractive interaction parameter $\Lambda(r_c)$, demonstrating that normalized critical temperatures collapse onto a near-universal relationship when expressed as a function of retained attractive energy. This result suggests that cutoff effects can be interpreted as a renormalization of the effective cohesive energy scale governing critical fluctuations. Dynamic analyses revealed pronounced critical slowing down, with relaxation times increasing strongly near the critical region and obeying finite-size scaling relationships with both system size and correlation length. Taken together, the results show that finite-size scaling, dynamic criticality, and cutoff-induced renormalization arise from a common fluctuation-driven mechanism. The proposed framework provides a physically transparent link between interaction-range truncation and emergent critical behavior and may be applicable to a broad range of molecular and soft-matter systems where truncated interaction potentials are routinely employed.

REFERENCE

Allen, M. P., & Tildesley, D. J. (2017). *Computer Simulation of Liquids*: Oxford University Press.

Binder, K. (1981). Finite size scaling analysis of ising model block distribution functions. *Zeitschrift für Physik B Condensed Matter, 43*(2), 119–140. doi:10.1007/BF01293604

Bruce, A. D., & Wilding, N. B. (1992). Scaling fields and universality of the liquid-gas critical point. *Physical Review Letters, 68*(2), 193–196. doi:10.1103/PhysRevLett.68.193

Caillol, J. M. (1998). Critical-point of the Lennard-Jones fluid: A finite-size scaling study. *The Journal of Chemical Physics, 109*(12), 4885–4893. doi:10.1063/1.477099

Das, S. K., Fisher, M. E., Sengers, J. V., Horbach, J., & Binder, K. (2006). Critical Dynamics in a Binary Fluid: Simulations and Finite-Size Scaling. *Physical Review Letters, 97*(2), 025702. doi:10.1103/PhysRevLett.97.025702

Das, S. K., Roy, S., & Midya, J. (2015). Coarsening in fluid phase transitions. *Comptes Rendus Physique, 16*(3), 303–315. doi:https://doi.org/10.1016/j.crhy.2015.03.006

Egami, T. (2020). Local Density Correlations in Liquids. *Frontiers in Physics, Volume 8 - 2020*. doi:10.3389/fphy.2020.00050

Fisher, M. E., & Barber, M. N. (1972). Scaling Theory for Finite-Size Effects in the Critical Region. *Physical Review Letters, 28*(23), 1516–1519. doi:10.1103/PhysRevLett.28.1516

Frenkel, D., & Smit, B. (2023). *Understanding Molecular Simulation: From Algorithms to Applications*: Academic Press.

Grossfield, A., Patrone, P. N., Roe, D. R., Schultz, A. J., Siderius, D. W., & Zuckerman, D. M. (2018). Best Practices for Quantification of Uncertainty and Sampling Quality in Molecular Simulations [Article v1.0]. *Living J Comput Mol Sci, 1*(1). doi:10.33011/livecoms.1.1.5067

Hansen, J. P., & McDonald, I. R. (2013). *Theory of Simple Liquids: with Applications to Soft Matter*: Academic Press.

Janeček, J. (2006). Long Range Corrections in Inhomogeneous Simulations. *The Journal of Physical Chemistry B, 110*(12), 6264–6269. doi:10.1021/jp056344z

Johnson, J. K., Zollweg, J. A., & Gubbins, K. E. (1993). The Lennard-Jones equation of state revisited. *Molecular Physics, 78*, 591–618. doi:10.1080/00268979300100411

Jones, J. E. (1924). On the Determination of Molecular Fields. II. From the Equation of State of a Gas. *Proceedings of the Royal Society of London Series A, 106*, 463–477. doi:10.1098/rspa.1924.0082

Kim, Y. C., Fisher, M. E., & Luijten, E. (2003). Precise Simulation of Near-Critical Fluid Coexistence. *Physical Review Letters, 91*(6), 065701. doi:10.1103/PhysRevLett.91.065701

Landau, D. P. B., K. (2014). *A Guide to Monte Carlo Simulations in Statistical Physics*: Cambridge University Press.

Mouritsen, O. G. (1989). Introduction to Phase Transitions and Critical Phenomena. By H. Eugene Stanley, Oxford University Press, Oxford, 1987. *International Journal of Quantum Chemistry*, *35*(4), 583–584. doi:https://doi.org/10.1002/qua.560350412

Nishimori, H., Ortiz, G., Nishimori, H., & Ortiz, G. (2010). Phase transitions and critical phenomena. In *Elements of Phase Transitions and Critical Phenomena* (pp. 0): Oxford University Press.

Onuki, A. (2002). *Phase Transition Dynamics*: Cambridge University Press.

Plimpton, S. (1995). Fast Parallel Algorithms for Short-Range Molecular Dynamics. *Journal of Computational Physics*, *117*(1), 1–19. doi:https://doi.org/10.1006/jcph.1995.1039

Potoff, J. J., & Panagiotopoulos, A. Z. (1998). Critical point and phase behavior of the pure fluid and a Lennard-Jones mixture. *The Journal of Chemical Physics*, *109*(24), 10914–10920. doi:10.1063/1.477787

Privman, V. (1990). *Finite Size Scaling And Numerical Simulation Of Statistical Systems*: World Scientific Publishing Company.

Rowlinson, J. S., & Widom, B. (2002). *Molecular Theory of Capillarity*: Dover Publications.

Smit, B. (1992). Phase diagrams of Lennard-Jones fluids. *The Journal of Chemical Physics*, *96*(11), 8639–8640. doi:10.1063/1.462271

Thol, M., Rutkai, G., Köster, A., Lustig, R., Span, R., & Vrabec, J. (2016). Equation of State for the Lennard-Jones Fluid. *Journal of Physical and Chemical Reference Data*, *45*(2). doi:10.1063/1.4945000

Thompson, A. P., Aktulga, H. M., Berger, R., Bolintineanu, D. S., Brown, W. M., Crozier, P. S., . . . Plimpton, S. J. (2022). LAMMPS - a flexible simulation tool for particle-based materials modeling at the atomic, meso, and continuum scales. *Computer Physics Communications*, *271*, 108171. doi:https://doi.org/10.1016/j.cpc.2021.108171

Torquato, S., & Stillinger, F. H. (2003). Local density fluctuations, hyperuniformity, and order metrics. *Physical Review E*, *68*(4), 041113. doi:10.1103/PhysRevE.68.041113

Verlet, L. (1967). Computer "Experiments" on Classical Fluids. I. Thermodynamical Properties of Lennard-Jones Molecules. *Physical Review*, *159*(1), 98–103. doi:10.1103/PhysRev.159.98

Wilding, N. B. (1995). Critical-point and coexistence-curve properties of the Lennard-Jones fluid: A finite-size scaling study. *Physical Review E*, *52*(1), 602–611. doi:10.1103/PhysRevE.52.602